Green Chemistry

PAPER

View Article Online
View Journal | View Issue

Cite this: *Green Chem.*, 2025, **27**, 6016

Tandem electrocatalytic benzylic alcohol oxidation and aldol condensation for efficient valuable α,β-unsaturated ketone production†

Yifan Yan,‡[a] Xi Cai,‡[a] Jiangrong Yang,‡[a] Yu Fu,[a] Qiwei Shi,[a] Pengjie Hao,[a] Hua Zhou,[a] Zhenhua Li,*[a,c] Mingfei Shao*[a,c] and Haohong Duan *[b,d,e]

α,β-Unsaturated ketones, crucial in organic synthesis and life sciences, are conventionally produced through aldol condensation of ketones and aldehydes. However, traditional synthesis methods involve high temperature, pressure, and the use of environmentally harmful solvents, hindering sustainable development. Herein, we present one-step electrosynthesis of benzylidene acetones and 2-methylenephenyl cyclohexanone *via* tandem reactions, by coupling electrooxidation of benzylic alcohols to the corresponding aldehyde, followed by aldol condensation between the aldehyde and the ketone. Selective formation of benzaldehydes is key to the tandem reaction and was achieved over a cubic oxide-supported gold catalyst (Au/CuO) as the anode, showing the ability to adsorb benzylic alcohols and generate the active adsorbed oxygen species (OH*) for selective oxidation. The tandem reaction strategy demonstrates its versatility in the synthesis of α,β-unsaturated ketones from benzyl alcohols with different substituents and acetone/cyclohexanone. As proof of concept, we constructed a flow electrolyzer and achieved continuous electrosynthesis of benzylidene acetone coupled with H_2 production at ampere-level current, delivering a benzylidene acetone productivity of 9.5 mmol h^{-1} and a H_2 productivity of 0.4 L h^{-1}. This study demonstrates the potential of coupling electrocatalysis and thermocatalysis in tandem, with implications for synthesis of more value-added chemicals.

Received 5th March 2025,
Accepted 14th April 2025

DOI: 10.1039/d5gc01155h

rsc.li/greenchem

Green foundation

1. This work describes a sustainable tandem electrocatalytic strategy for one-step synthesis of α,β-unsaturated ketones, eliminating the need for high temperatures, high pressures, and hazardous organic solvents traditionally required for aldol condensation. The use of renewable electricity further enhances its green chemistry potential.
2. The electrocatalytic oxidation of aromatic alcohols over an Au/CuO catalyst achieves high benzylidene acetone productivity (9.5 mmol h^{-1}) with 84% selectivity, while simultaneously producing 0.4 L h^{-1} of H_2 as a valuable byproduct. This approach demonstrates a high AE (89%) and a low *E*-factor (0.71), making it a more sustainable alternative.
3. Further research could focus on renewable feedstock integration, optimizing catalyst durability, and scaling up flow electrolyzers to industrial levels, which may improve efficiency and overall sustainability.

Introduction

α,β-Unsaturated carbonyl compounds are important intermediates in basic organic synthesis and life science industries. In particular, α,β-unsaturated ketones are critical fine chemicals that are widely employed in flavors, fragrances, pesticides and food additives.[1–4] These compounds are commercially produced by aldol condensation reactions between aldehydes and ketones in one reactor, and the aldehydes are synthesized *via* alcohol oxidation in another reactor, and thus multiple reactors are required, leading to tedious processing (Scheme 1a).[5–7] Although some pioneering works reported the synthesis of α,β-unsaturated ketones in one pot *via* tandem

[a]*State Key Laboratory of Chemical Resource Engineering, Beijing University of Chemical Technology, Beijing 100029, P. R. China. E-mail: LZH0307@mail.buct.edu.cn, shaomf@mail.buct.edu.cn*
[b]*Department of Chemistry, Tsinghua University, 30 Shuangqing Rd, Haidian Qu, Beijing 100084, P. R. China. E-mail: hhduan@mail.tsinghua.edu.cn*
[c]*Quzhou Institute for Innovation in Resource Chemical Engineering, Quzhou 324000, P. R. China*
[d]*Haihe Laboratory of Sustainable Chemical Transformations, Tianjin 300192, China*
[e]*Engineering Research Center of Advanced Rare Earth Materials (Ministry of Education), Department of Chemistry, Tsinghua University, Beijing 100084, China*
†Electronic supplementary information (ESI) available. See DOI: https://doi.org/10.1039/d5gc01155h
‡These authors contributed equally to this work.

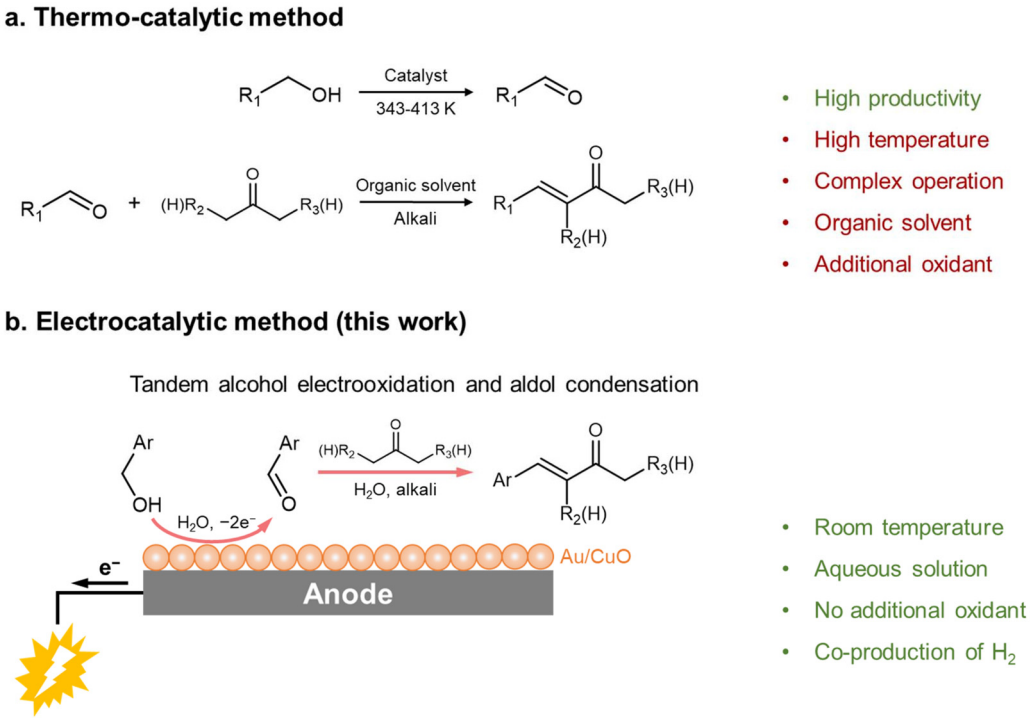

Scheme 1 Tandem coupling of alcohol electrooxidation with aldol condensation. Ar: aromatic substituent.

aerobic oxidation of alcohols and aldol condensation with ketones,[8–11] elevated temperatures (for example, 413 K), organic solvents and external oxidants (oxygen) are necessary (Scheme 1a), calling for a more sustainable approach that is operated under mild conditions.

Electrocatalytic synthesis is regarded as a promising approach for producing high-value-added compounds, thanks to its mild electrochemical reaction conditions and the possibility to integrate renewable electricity.[12–16] Very recently, tandem electrocatalysis has been reported for the production of value-added chemicals, by combining electro- and thermo-catalytic processes.[17–21] For example, Zhang and coworkers reported electrosynthesis of cyclohexanone oxime *via* tandem electroreduction of NO_2^- to NH_2OH* (as an intermediate) and the cyclohexanone-hydroxylamine reaction.[21] Zou and co-workers, in a tandem electrochemical-chemical-electrochemical reaction, coupled the electroreduction of NO_3^- to NH_2OH with its chemical reaction with pyruvic acid to produce pyruvic oxime, which was electroreduced to alanine.[18] In addition, our group reported the electrosynthesis of lactic acid from glycerol, a byproduct of biodiesel, using tandem reactions. These reactions include the electrooxidation of glycerol to glyceraldehyde or dihydroxyacetone intermediates, followed by base-catalyzed dehydration and the Cannizzaro rearrangement, ultimately producing the biodegradable plastic monomer lactic acid.[17]

Inspired by previous achievements in tandem reactions, we envisaged that high selectivity for electrooxidation of alcohols to aldehydes and efficient aldol condensation are two key points for one-step synthesis of α,β-unsaturated ketones.[10,22] Herein, we report the selective electrooxidation of benzylic alcohols to the corresponding benzaldehydes using a cooperative Au/CuO catalyst, followed by spontaneous aldol condensation between the benzaldehyde and a ketone (acetone and cyclohexanone) in an alkaline environment, efficiently producing the corresponding α,β-unsaturated ketones in one step (Scheme 1b). To maximize electron economy and energy efficiency, we further integrated the electrosynthesis of benzylidene acetone at the anode with its electroreduction at the cathode to a saturated ketone, 4-phenyl-butane-2-one. This study underscores the great potential of coupling electro- and thermo-catalysis in a tandem manner, paving the way for enhanced synthesis of valuable chemicals.

Results and discussion

Characterization of the Au/CuO catalyst

For the synthesis of α,β-unsaturated ketones *via* tandem electrocatalytic alcohol oxidation and aldol condensation, achieving selective electrooxidation of alcohols to their corresponding aldehydes is absolutely essential. CuO has been proven to be an efficient catalyst for the selective oxidation of alcohols to aldehydes in thermocatalysis,[23–25] photocatalysis[26] and electrocatalysis.[27] For example, Sun and co-workers reported the electrooxidation of alcohols (including aromatic alcohols, furfuryl alcohol and 4-pyridine methanol) to the corresponding aldehydes with high selectivity (>85%) over a

CuO catalyst in alkaline solution. However, the current density for electrooxidation of alcohols on CuO itself is low (<10 mA cm^{-2}), which hinders further applications.[27] In a recent study,[28] we demonstrated that reactive oxygen species (typically OH*) are generated over Au at low potentials (<1.2 V *vs.* RHE), enabling oxidative dehydrogenation of alcohols. Moreover, Au could adsorb benzene rings *via* π bonding between the occupied Au 5d orbital and the unoccupied π* orbital of the benzene ring, which is anticipated to enhance reactant adsorption and thus increase the current density. Therefore, we envisaged constructing an Au/CuO cooperative catalyst to combine the high selectivity of CuO with the high activity of Au, thereby achieving selective oxidation of alcohols to aldehydes at high current densities.

For the preparation of the Au/CuO catalyst, CuO nanosheets were first grown on Ni foam *via* a hydrothermal method, followed by a calcination process at 453 K. Then, Au nanoparticles (NPs) were electrodeposited on CuO to obtain Au/CuO (Fig. 1a). Pure CuO nanosheets and Au NPs on Ni foam were also synthesized with the same methods and act as reference samples (Fig. S1, ESI†). Fig. S2 (ESI)† shows the X-ray diffraction (XRD) patterns of CuO and Au/CuO. The diffraction peaks at 35.3° and 38.5° are attributed to the (002) and (111) planes of CuO, respectively (JCPDS #44-0706). The peaks at 44.5° and 51.8° are attributed to the Ni foam substrate (JCPDS #04-0850). For Au/CuO, the peak at 38.2° is broader than that of CuO, which can be attributed to the (111) plane of face-centered cubic Au (JCPDS #04-0784). Scanning electron microscope (SEM) images (Fig. 1b) show that the CuO nanosheets are vertically aligned on the Ni foam, with an average thickness of ~20 nm and a diameter of 300–400 nm. The energy-dispersive spectroscopy (EDS) mapping results show that Au NPs are uniformly distributed on the surface of the CuO nanosheets with an average diameter of 15 nm (Fig. 1c). High-resolution transmission electron microscopy (HRTEM) images show that both Au and CuO are well crystallized and exposed to the (111) plane (Fig. S3, ESI†).

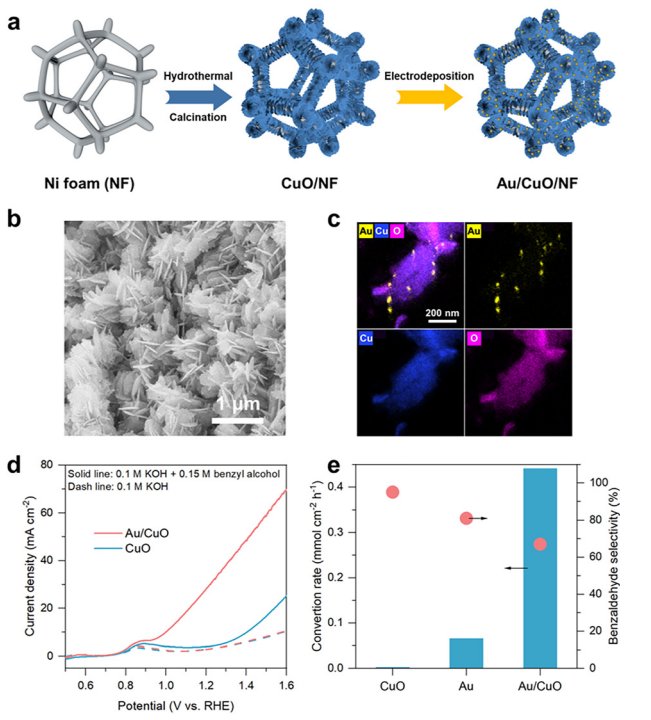

Fig. 1 (a) Schematic illustration of the synthesis of the Au/CuO catalyst. (b) SEM image of Au/CuO. (c) STEM mapping of Au/CuO. (d) LSV curves in 0.1 M KOH (dashed line) and in 0.1 M KOH with 0.15 M benzyl alcohol (solid line) at a scan rate of 10 mV s^{-1} over different catalysts. (e) Conversion rate of benzyl alcohol and the corresponding selectivity for benzaldehyde at 1.16 V *vs.* RHE over different catalysts.

Selective electrocatalytic oxidation of benzyl alcohol

Benzyl alcohol oxidation to benzaldehyde was selected as a model reaction to verify the feasibility of tandem selective electrocatalytic alcohol oxidation and aldol condensation to produce α,β-unsaturated ketones. The electrochemical tests were conducted in a three-electrode configuration in a glass cell. As shown in Fig. 1d, in 0.1 M KOH, both CuO and Au/CuO exhibit two oxidation waves in the anodic direction, which are attributed to the oxidation of Cu^0/Cu^{1+} to Cu^{2+} (from 0.7 to 0.9 V *vs.* RHE) and the occurrence of the oxygen evolution reaction (OER, from ~1.35 V *vs.* RHE).[29] After adding 0.15 M benzyl alcohol (solid line), CuO shows low performance for benzyl alcohol oxidation before 1.3 V *vs.* RHE. The current density increased rapidly after 1.35 V *vs.* RHE, corresponding to the oxidation of benzyl alcohol by CuOOH (generated at ~1.35 V *vs.* RHE).[30,31] In contrast, Au/CuO shows an obvious benzyl alcohol oxidation current that starts from ~0.9 V *vs.* RHE, much lower than the CuOOH formation potential, suggesting that benzyl alcohol oxidation over Au/CuO at this low potential may be facilitated by Au. We thus investigated the performance of Au on which the oxidation of benzyl alcohol begins at ~0.7 V *vs.* RHE (Fig. S4, ESI†), confirming that the lower onset potential of benzyl alcohol oxidation over Au/CuO is due to Au, rather than CuO. Note that the current density of Au/CuO is significantly higher than that of pure Au and CuO. These results indicate that the cooperative catalyst strategy can enhance the activity of the electrode for the electrooxidation of benzyl alcohol, with Au serving as the primary catalytic site.

We then investigated the effect of oxidation potential on benzyl alcohol oxidation over Au/CuO *via* chronoamperometric (CA) tests. The reaction products were quantitatively analyzed by high-performance liquid chromatography (HPLC). As shown in Fig. S5 (ESI),† the conversion rate of benzyl alcohol over Au/CuO increases gradually with the increase of the oxidation potential from 0.96 to 1.56 V *vs.* RHE, reaching its highest at 1.56 V *vs.* RHE with a rate of 0.92 mmol cm^{-2} h^{-1}. In contrast, benzaldehyde selectivity decreases with the increase of reaction potentials (from 73% to 47%) due to the formation of benzoic acid *via* overoxidation (Fig. S5(c) and S6, ESI†). By collectively considering the reaction rate and benzaldehyde selectivity, 1.16 V *vs.* RHE was selected as the optimal reaction potential. Additionally, we observed that reducing the KOH concentration

enhances benzaldehyde selectivity (Fig. S7, ESI†); however, it markedly decreases the reaction rate. Considering both factors, we selected 0.1 M KOH as the electrolyte.

We then compared the performance of electrooxidation of benzyl alcohol over the Au, CuO and Au/CuO catalysts. As shown in Fig. 1e, CuO exhibits a high benzaldehyde selectivity of 95% at 1.16 V *vs.* RHE, while its benzyl alcohol conversion rate is only 0.0024 mmol cm^{-2} h^{-1}. The benzyl alcohol conversion rate over Au reaches 0.066 mmol cm^{-2} h^{-1}, together with a benzaldehyde selectivity of 81%. On Au/CuO, the conversion rate of benzyl alcohol achieves 0.44 mmol cm^{-2} h^{-1}, which is 6.7-fold and 183-fold higher than that on Au and CuO, respectively, while maintaining a relatively good benzaldehyde selectivity of 67%. We also examined the role of nickel foam, as shown in Fig. S8 (ESI),† confirming that Ni foam functions solely as a substrate in this study.

One-step electrosynthesis of benzylidene acetone

Based on the promising performance of Au/CuO for the selective electrooxidation of benzyl alcohol to benzaldehyde, we then investigated the electrosynthesis of benzylidene acetone directly from benzyl alcohol and acetone. Benzylidene acetone is a typical α,β-unsaturated ketone that is widely used in synthetic spices, pesticides, and galvanized brighteners, which can be synthesized *via* aldol condensation between benzaldehyde and acetone under an alkaline environment.[10] Since the electrooxidation of benzyl alcohol to benzaldehyde was performed in an alkaline electrolyte (0.1 M KOH), we thought to add acetone to the electrolyte, which may react with the generated benzaldehyde intermediate from benzyl alcohol *via* spontaneous aldol condensation, consequently producing benzylidene acetone in one step.

To demonstrate this assumption, we investigated the effect of acetone addition to the electrolyte on the electrocatalytic performance of Au/CuO. As shown in Fig. 2a, the current density for the OER and benzyl alcohol oxidation over Au/CuO remained nearly unchanged after acetone addition, indicating that acetone is stable and does not participate in the electrocatalytic process. The slight decrease in current may be due to increased electrolyte resistance. Previous studies have also shown that acetone is stable under alkaline conditions and does not polymerize in a short time.[32]

We subsequently verified the spontaneous aldol condensation between benzaldehyde and acetone in 0.1 M KOH. As shown in Fig. S9 (ESI),† 0.15 M benzaldehyde spontaneously converts entirely to benzylidene acetone with acetone within 20 minutes, significantly faster than benzyl alcohol electrooxidation (0.44 mmol cm^{-2} h^{-1} over Au/CuO), suggesting that the *in situ* produced benzaldehyde can be quickly consumed by reacting with acetone.

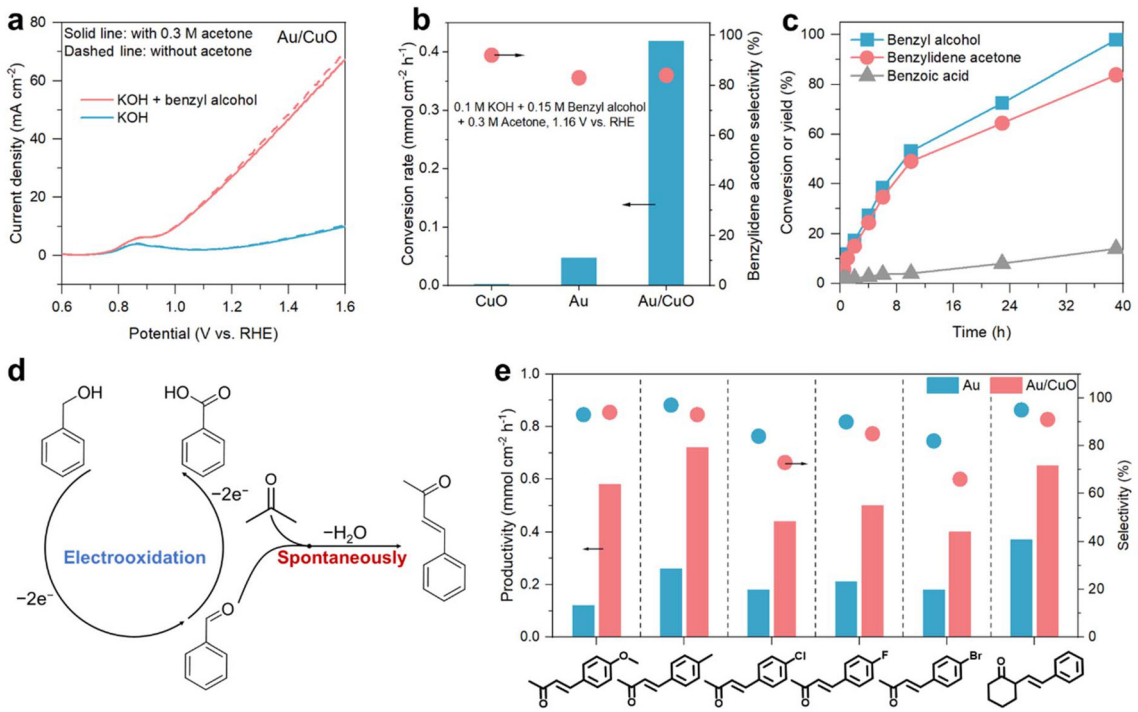

Fig. 2 (a) Dashed line: LSV curves of Au/CuO in 0.1 M KOH or 0.1 M KOH with 0.15 M benzyl alcohol. Solid line: LSV curves of Au/CuO in 0.1 M KOH with 0.3 M acetone or 0.1 M KOH with 0.15 M benzyl alcohol and 0.3 M acetone. (b) Benzyl alcohol conversion rate and benzylidene acetone selectivity over different catalysts. (c) Kinetic curves for benzyl alcohol oxidation over Au/CuO at 1.16 V *vs.* RHE. (d) Proposed reaction mechanisms. (e) Substrate expansion. The first five reactions were performed in 0.1 M KOH with 0.15 M benzyl alcohols with different substituents (−Cl, −F, −Br, $-CH_3$, and $-OCH_3$) and 0.3 M acetone at 60 °C at 1.16 V *vs.* RHE. The sixth reaction was performed in 0.1 M KOH with 0.15 M benzyl alcohol and 0.3 M cyclohexanone at room temperature at 1.16 V *vs.* RHE.

We then carried out CA measurements at 1.16 V *vs.* RHE to verify the feasibility of electrooxidation of benzyl alcohol to produce benzylidene acetone. As shown in Fig. 2b and S10 (ESI),† benzylidene acetone was successfully synthesized during the benzyl alcohol oxidation process in 0.1 M KOH, and the selectivities of benzylidene acetone over Au, CuO and Au/CuO are all higher than 80% (the byproduct is benzoic acid). Notably, for Au/CuO, the selectivity of benzylidene acetone in the presence of acetone (84%) is significantly higher than that of benzaldehyde without acetone (67%), which may be due to the facile aldol condensation reaction between acetone and benzaldehyde, lowering the amount of benzaldehyde being oxidised to benzoic acid. In terms of reaction rate, Au/CuO shows a benzylidene acetone productivity of 0.35 mmol cm^{-2} h^{-1}, which is 9-fold and 159-fold higher than that of Au and CuO, respectively. Moreover, the yield of benzylidene acetone reached 84% when the conversion of benzyl alcohol was higher than 98% (Fig. 2c), suggesting that the reaction strategy has potential for practical application that requires high conversion.

According to the above experimental results, we propose the following reaction path for the benzylidene acetone electrosynthesis. As shown in Fig. 2d, benzyl alcohol is first oxidized to the benzaldehyde intermediate *via* an electrocatalytic process. The generated benzaldehyde intermediate rapidly reacts with the excess acetone in the solution, producing benzylidene acetone through aldol condensation while preventing the overoxidation of benzaldehyde. For the stability of the Au/CuO catalyst, the preliminary results show that the conversion rate of benzyl alcohol and the selectivity of benzylidene acetone were largely maintained after 10 batches (overall 10 h; Fig. S11, ESI†), together with the preservation of the original nanosheet structure (Fig. S12, ESI†), demonstrating high stability.

To demonstrate the generality of this one-step electrosynthesis of α,β-unsaturated ketones from alcohols, benzyl alcohols with diverse substituents (–Cl, –F, –Br, $–CH_3$, and $–OCH_3$) were examined. The electrooxidation reactions were performed at 60 °C to guarantee the full dissolution of alcohols in 0.1 M KOH (Fig. S13, ESI†). As shown in Fig. 2e, benzylidene acetones with diverse substituents (–Cl, –F, –Br, $–CH_3$, and $–OCH_3$) were successfully synthesized in 0.1 M KOH with 0.3 M acetone (Fig. S14, ESI†), together with high selectivity (>60%). Additionally, Au/CuO exhibits a 1.8 to 4.8-fold enhancement in productivity compared with Au for these α,β-unsaturated ketones, indicating the excellent performance of Au/CuO to produce α,β-unsaturated ketones. Moreover, we replaced acetone with cyclohexanone and successfully obtained 2-phenylmethylene cyclohexanone from benzyl alcohol in one step with a selectivity of 91% (Fig. S15, ESI†), further demonstrating the generality of this strategy.

Promoting the generation of OH* over Au/CuO

The above experimental results reveal that the performance of benzyl alcohol oxidation over Au/CuO is significantly superior to that of pure Au and pure CuO. Initially, to investigate the catalytically active site in Au/CuO, methionine was added in the chronopotentiometry test (10 mA cm^{-2}) to poison Au. As shown in Fig. 3a, the reaction potential of Au rapidly increased by more than 0.6 V *vs.* RHE, implying that Au is rapidly poisoned and deactivated by methionine. For CuO, the reaction potential did not change significantly after adding methionine, indicating that methionine has little effect on CuO. For Au/CuO, the reaction potential is initially lower than that of Au, suggesting higher activity of the cooperative catalyst. However, upon addition of methionine, its potential rapidly increases to a level similar to that of CuO, confirming that Au plays the catalytic role in Au/CuO.

To further elucidate the mechanism behind the high performance of Au/CuO, we calculated the turnover frequency (TOF) value to investigate the intrinsic activity of Au.[14] As shown in Fig. S16 (ESI),† the TOF value of Au/CuO is calculated to be 0.34 s^{-1} at 1.16 V *vs.* RHE, which is 4.8-fold higher than that of pure Au, indicating that the excellent activity of Au/CuO stems from the synergistic effect of Au and CuO. Due to the much higher electrochemically active surface area (ECSA) of Au/CuO compared to Au (Fig. S17, ESI†), we normalized the conversion rate of benzyl alcohol by the ECSA to further exclude the possibility that the excellent performance of Au/CuO arises from its higher ECSA. As shown in Fig. S18 (ESI),† the normalized conversion rate of benzyl alcohol over Au/CuO is 1.9 times higher than that of Au, ruling out the possibility that the high activity of Au/CuO is from its nanosheet structure.

Previous studies have shown that in alcohol electrooxidation, Au adsorbs OH^- to generate OH*, thereby oxidizing the alcohol molecule for dehydrogenation.[15] We first compared the OH^- adsorption ability of Au and Au/CuO *via* zeta potential tests.[33] As shown in Fig. 3b, Au/CuO shows a lower zeta potential value than Au, showing that Au/CuO can adsorb more OH^- in the inner Helmholtz layer. Then we investigated the ability of Au and Au/CuO to produce OH*. To ensure accurate detection of the OH* signal, Au and Au/CuO were deposited onto a glass carbon electrode for the electrochemical tests. As shown in Fig. 3c, during the anodic scan in 0.1 M KOH, Au exhibits two oxidation peaks, which are attributed to the adsorption of OH^- to form Au–OH* (from ~0.85 V *vs.* RHE) and its further oxidation to AuO_x.[34] For Au/CuO, three oxidation peaks were observed. The first and second anodic peaks are attributed to the oxidation of Cu^0 to Cu^{1+} (from 0.5 to 0.7 V *vs.* RHE) and its further oxidation to Cu^{2+} (from 0.7 to 0.9 V *vs.* RHE).[35–37] The intensity of the third oxidation peak, attributed to Au–OH*, is significantly higher than that of pure Au, indicating that the ability to generate OH* on Au/CuO is stronger than on Au.

After adding 0.15 M benzyl alcohol, the oxidation current of both Au and Au/CuO begins to increase from ~0.8 V *vs.* RHE (Fig. 3c inset), which is due to the oxidation of benzyl alcohol by Au–OH*.[38] Note that the current density with Au/CuO is significantly higher than that with Au, demonstrating the better performance of Au/CuO for benzyl alcohol oxidation. The oxidation current of Au and Au/CuO diminishes at ~1.45 V *vs.* RHE because of the formation of AuO_x.

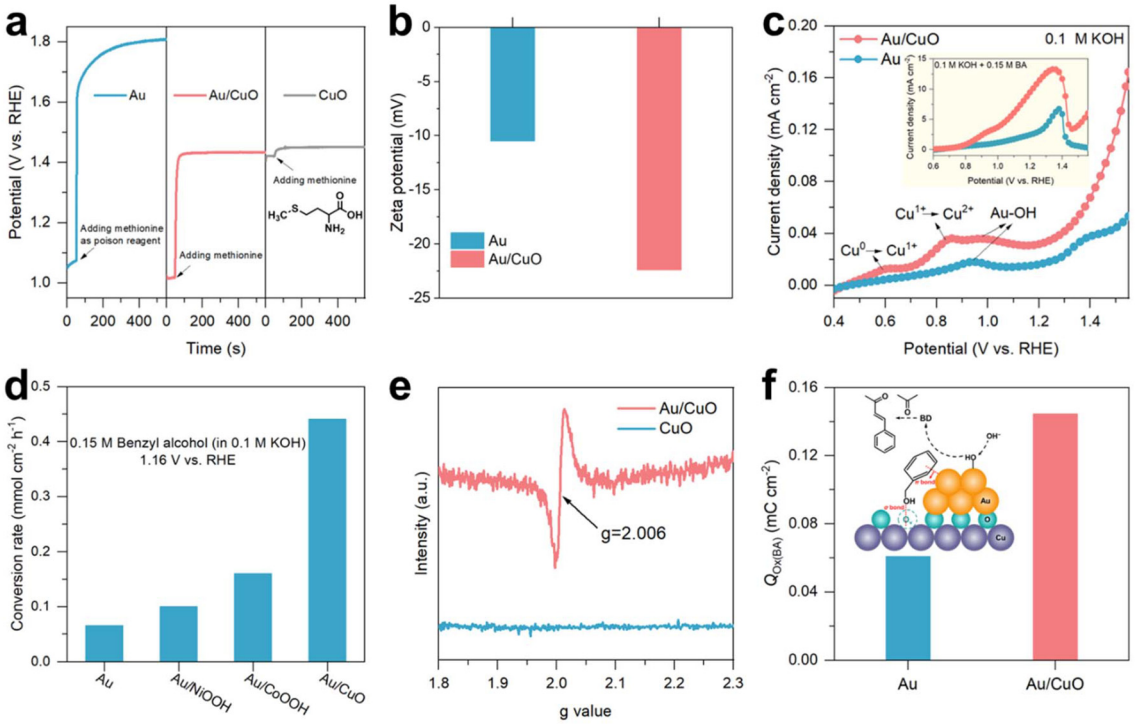

Fig. 3 (a) Chronopotentiometry curves of different catalysts in 0.1 M KOH with 0.15 M benzyl alcohol at 10 mA cm^{-2} (methionine was added at 50 s). (b) Zeta potentials of different samples. (c) LSV curves of glassy carbon electrodes supported with Au/CuO and Au in 0.1 M KOH and 0.1 M KOH with 0.15 M benzyl alcohol (inset). (d) Conversion rates of benzyl alcohol over different samples. (e) Room temperature EPR spectra of CuO and Au/CuO. (f) Values of the oxidation charges ($Q_{Ox(BA)}$) for adsorbed BA over Au/CuO and Au. Inset: schematic illustration of the synergistic effect in Au/CuO. Abbreviation: benzaldehyde (BD).

According to previous reports, the electron deficiency of Au is theoretically more conducive to adsorbing OH^-, which may be more beneficial for generating OH*.[14,39,40] Therefore, we investigated the electronic structure of Au/CuO using X-ray photoelectron spectroscopy (XPS). As shown in Fig. S19 (ESI),† the peaks of Au 4f over Au/CuO shift ~0.2 eV towards higher energy compared to Au. Conversely, the peaks of Cu 2p in Au/CuO shift negatively by ~0.2 eV relative to Cu. Previous studies have shown that loading Au onto other oxyhydroxides would also transfer electrons from Au to oxyhydroxides, thereby forming electron-deficient Au, which could promote OH* production and thus improve alcohol oxidation activity.[28] To verify the specificity of Au/CuO, we constructed Au/NiOOH and Au/CoOOH catalysts and investigated their performance. XPS results show that there is an electron transfer at Au/NiOOH and Au/CoOOH interfaces from Au to NiOOH/CoOOH, forming electron-deficient Au (Fig. S20, ESI†). However, the performance of Au/CuO is still significantly better than that of the other catalysts (Fig. 3d and S21, ESI†), implying that the CuO support also plays a key role in the superior performance of Au/CuO.

Enhanced adsorption of benzyl alcohol at the Au/CuO interface

We then paid our attention to studying the role of CuO in Au/CuO. The XPS results show that CuO at the Au/CuO interface is reduced (by taking electrons from Au; Fig. S19, ESI†), which may be accompanied by the generation of oxygen vacancies. Hence, electron paramagnetic resonance (EPR) was conducted to verify the presence of oxygen vacancies in Au/CuO. As shown in Fig. 3e, the EPR spectrum of Au/CuO shows a strong EPR signal at a *g* value of 2.006, attributed to electrons trapped in oxygen vacancies.[41] Previous works have demonstrated that oxygen vacancies can be recognized as electrophilic sites for the adsorption and activation of C=O/C–OH bonds in organics.[42,43]

We subsequently investigated the benzyl alcohol adsorption ability of Au/CuO and pure Au. Open circuit potential (OCP) measurements were carried out to detect the change in organic adsorbent content in the inner Helmholtz layer of the electrode.[44] As shown in Fig. S22 (ESI),† the OCP changes of Au/CuO are more obvious than those of Au (0.44 *vs.* 0.37 V) when 0.05 M benzyl alcohol was injected, indicating that more benzyl alcohol molecules are adsorbed in the inner Helmholtz layer of Au/CuO. The enhanced adsorption of benzyl alcohol over Au/CuO was also examined by electrochemical adsorbate-stripping measurements (see the ESI† for experimental details), and the oxidation charges of benzyl alcohol ($Q_{Ox(BA)}$) can be used to quantify the amount of adsorbed benzyl alcohol (Fig. S23, ESI†).[45] As shown in Fig. 3f, the $Q_{Ox(BA)}$ of Au/CuO is 2.4-fold higher than that of pure Au, suggesting that Au/CuO has a stronger ability to adsorb benzyl alcohol.

Therefore, the significantly enhanced reaction rate of benzyl alcohol oxidation on Au/CuO can be attributed to the synergistic effect of Au and CuO to enhance the generation of OH* and the adsorption of benzyl alcohol (Fig. 3f inset).

Spin-polarized density functional theory studies

Spin-polarized density functional theory (DFT) calculations were performed to reveal the synergistic effect of Au/CuO in the oxidation reaction of benzyl alcohol to benzaldehyde and the subsequent aldol condensation reaction between benzaldehyde and acetone to produce benzylidene acetone. Detailed information for model construction and computational methods is described in Note S1.† According to the XRD patterns (Fig. S2, ESI†) and HRTEM images (Fig. S3, ESI†), the Au(111) surface and the CuO(111) surface were selected as the exposed facets to construct models, which have also been reported to be one of the active surfaces of Au and CuO.[46] The formation energies of oxygen vacancies with various coordination numbers (VO_{3C} and VO_{4C}) were calculated and are displayed in Fig. S24 (ESI),† and the model of the Au_{10} cluster loading on the CuO-VO_{3C} model was determined to represent Au/CuO.

The Gibbs free energy changes (ΔG_{OH^*}) for the generation of the active oxygen species (OH*) on Au and Au/CuO were calculated for different geometric sites (Fig. 4a); the corresponding models are shown in Fig. S25 (ESI).† The ΔG_{OH^*} values of OH* at the vertex site on Au/CuO and Au are lower than that at the edge site, which is attributed to the smaller coordination number of the vertex site. Moreover, the ΔG_{OH^*} of OH* at the vertex site on Au/CuO is 0.67 eV, which is lower than that on Au (1.29 eV). The Hirshfeld charge analysis indicated that electrons transferred from Au atoms to CuO, result-

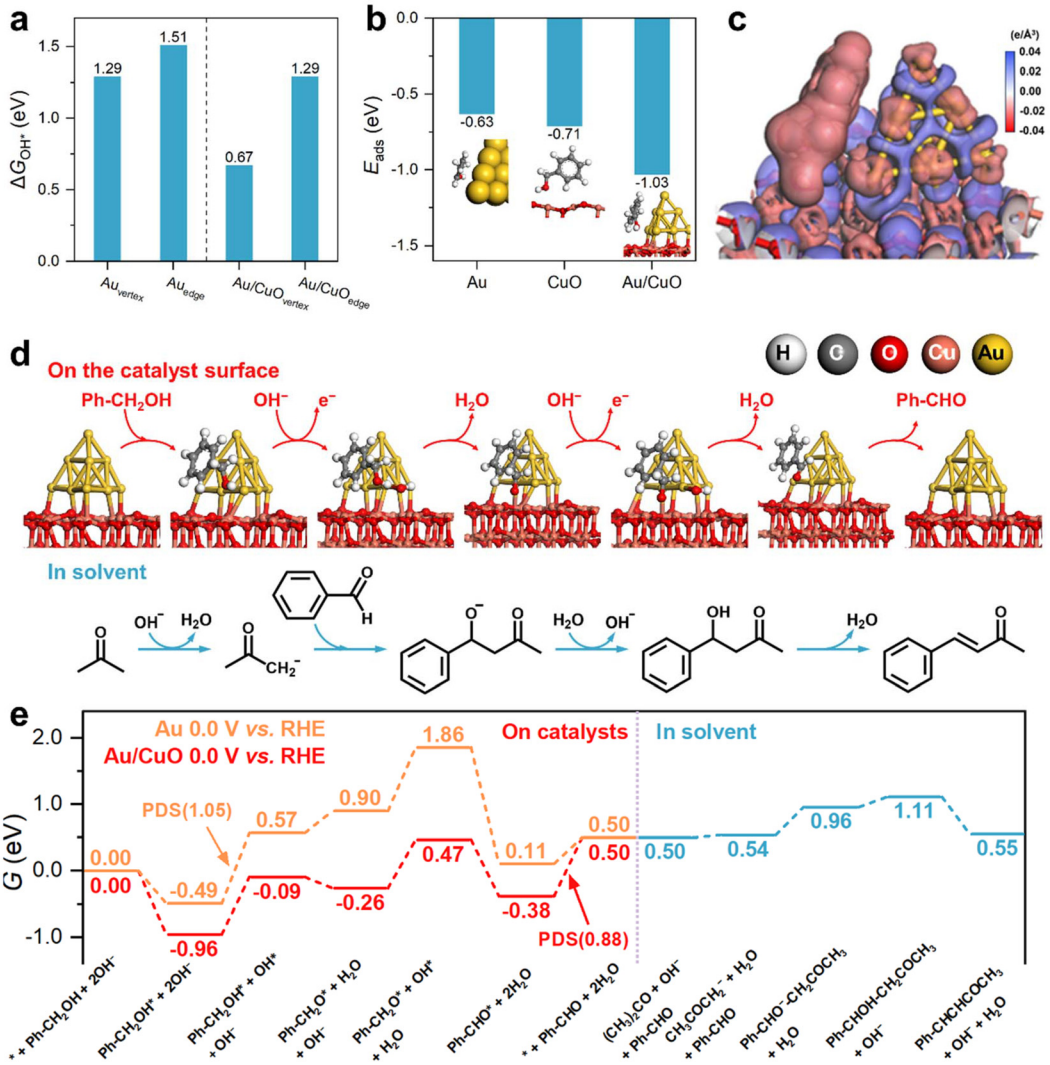

Fig. 4 (a) The Gibbs free energy change for the generation of OH* on Au and Au/CuO at the vertex and edge sites of Au clusters. (b) The adsorption energy of benzyl alcohol on different samples. (c) The charge density difference plots for benzyl alcohol adsorbed on Au/CuO. The red (blue) distribution corresponds to charge accumulation (depletion). (d) Schematic illustration and (e) Gibbs free energy diagrams for benzyl alcohol oxidation to benzaldehyde on Au and Au/CuO and aldol condensation reaction of benzaldehyde with acetone. The color for each element is labeled.

ing in Au atoms at the Au/CuO interface being more electron-deficient than those in pure Au (Fig. S26, ESI†), consistent with the XPS results. As a result, the nucleophilic molecule H_2O and the ions OH^- are adsorbed preferentially on electron-deficient Au clusters in Au/CuO to generate OH*.

Moreover, the energies of benzyl alcohol adsorption (E_{ads}) on Au, CuO, and Au/CuO were calculated and are displayed in Fig. 4b. The E_{ads} of benzyl alcohol on Au/CuO is −1.03 eV, which is higher than that on Au (−0.63 eV) and CuO (−0.71 eV), demonstrating that the Au/CuO interface is more favorable for adsorbing benzyl alcohol. The analysis of the density of states (DOS) (Fig. S27, ESI†) and charge density difference (Fig. S28, ESI†) revealed that benzyl alcohol is chemically adsorbed on Au/CuO *via* a covalent σ bond between the 2p orbital of the O atom in the hydroxyl group of benzyl alcohol and the 3d orbital of Cu in Au/CuO and a π bond between the unoccupied π^* orbital of benzyl alcohol and the occupied Au 5d orbital of the Au cluster, thereby strengthening the adsorption of benzyl alcohol at the Au/CuO interface and thus improving the reaction rate (Fig. 4c).[28]

In addition, we calculated the Gibbs free energy diagrams of the whole reaction process, including the electrooxidation process of benzyl alcohol to benzaldehyde on the catalyst surface and aldol condensation to generate benzylidene acetone in solvent (Fig. 4d). As shown in Fig. 4e, the benzyl alcohol is first adsorbed at the Au/CuO interface with a ΔG of −0.96 eV, which is higher than that on Au (−0.49 eV). Then, the nucleophilic OH* is generated on Au clusters for Au/CuO and Au, which attacks Ph-CH_2OH* to generate one molecule of H_2O and the adsorbed radical Ph-CH_2O*. Afterwards, another nucleophilic OH* is also generated on the Au clusters and reacts with Ph-CH_2O* to generate Ph-CHO* and H_2O. Then, the benzaldehyde is desorbed from the catalyst into the solvent, followed by aldol condensation with acetone to produce benzylidene acetone. For the electrooxidation process over Au/CuO and Au, the potential-determining steps (PDS) are the benzaldehyde desorption and the generation of OH*, respectively. According to the Brønsted–Evans–Polanyi relation,[47] the ΔG for the benzaldehyde desorption from Au/CuO is lower than the ΔG_{OH^*} of OH* on Au (0.88 *vs.* 1.05 eV), which means that the activation energy barrier for this elementary reaction is lower on Au/CuO. Therefore, the theoretical reaction rate is higher on Au/CuO than on Au at the same potential. Note that although the desorption energy of benzaldehyde on Au/CuO is slightly higher than that on Au (0.88 *vs.* 0.39 eV), the desorption can be overcome by the kinetic energy of benzaldehyde at room temperature, especially under strong stirring, to participate in the subsequent aldol condensation process.

Electrosynthesis of benzylidene acetone in a flow electrolyzer

To assess the catalytic efficacy for the electrosynthesis of benzylidene acetone in a more practical scenario, we conducted a two-electrode test employing a homemade membrane-free flow electrolyzer using the Au/CuO catalyst as the anode and Ni foam as the cathode (working area: 30 cm^2; Fig. 5a inset and S29, ESI†). The LSV curves in Fig. 5a reveal a noticeable reduction in the onset potential for the benzyl alcohol oxi-

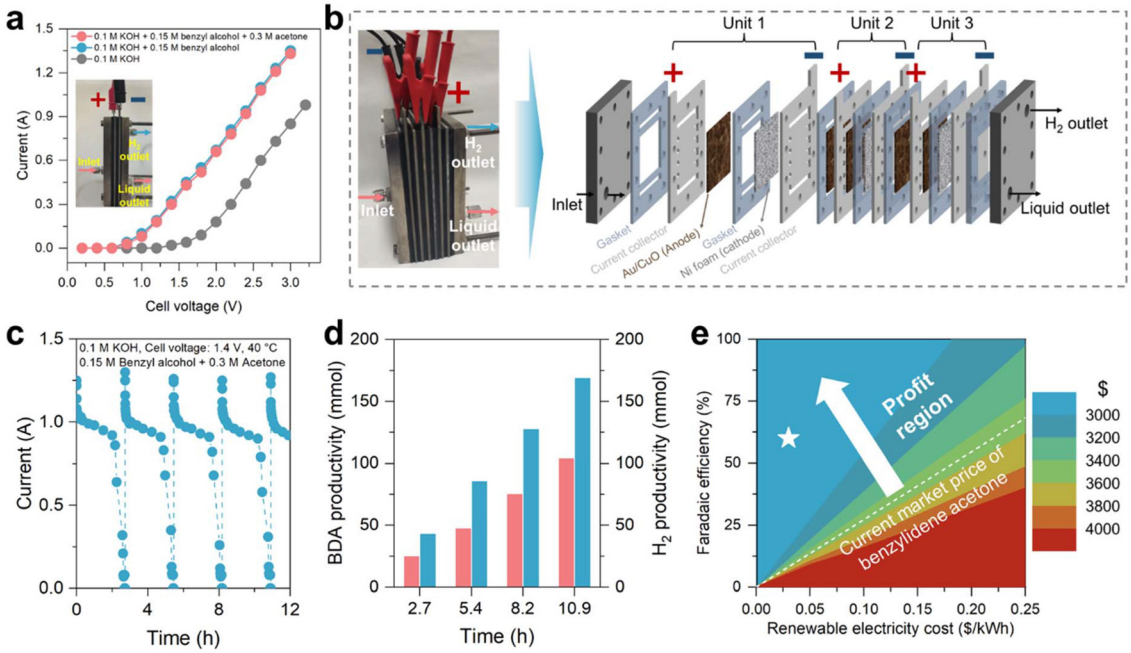

Fig. 5 (a) LSV curves of Au/CuO in the membrane-free flow electrolyzer with a single cell (working area: 30 cm^2). The inset shows the photograph of the single-unit membrane-free flow electrolyzer. (b) Photograph and schematic illustration of the stacked membrane-free flow electrolyzer with three units (working area: 150 cm^2). (c) *I-t* curve of Au/CuO in the stacked electrolyzer. (d) Productivities of benzylidene acetone (BDA) and the corresponding H_2 productivity. (e) TEA of the levelized cost of benzylidene acetone electrosynthesis.

dation reaction (denoted as BOR) compared to water splitting (from 1.6 V to 0.8 V), indicating the favorability of the BOR over the OER. Additionally, the current exhibits minimal alteration subsequent to the introduction of acetone, akin to the trend observed in Fig. 2a. This again suggests that acetone maintains stability under the reaction conditions and does not engage in the electrocatalytic process.

Subsequently, we assembled a stacked membrane-free flow electrolyzer consisting of three units with a total working area of 150 cm^2 (Fig. 5b). CA measurements were performed to evaluate the electrosynthesis of benzylidene acetone at industrially relevant current. The electrochemical tests were performed at a constant cell voltage of 1.4 V to exclude the influence of the OER. Moreover, an intermittent potential (IP) strategy, proposed in our previous work,[17] was employed to stabilize the catalyst that keeps the absolute current at a high level during long-term testing. As depicted in Fig. 5c and d, the stacked electrolyzer exhibited an absolute current of ~1 A at 1.4 V, achieving a benzylidene acetone productivity of 103.4 mmol in 10.9 h (0.06 mmol cm^{-2} h^{-1}) with relatively high selectivity (75%) and FE (60%) (Fig. S30†). Concurrently, cathodic H_2 productivity reached 0.4 L h^{-1} with an energy consumption of 3.2 kWh Nm^{-3} H_2, significantly lower than the advanced water electrolysis system (~4.2 kWh Nm^{-3} H_2).[48]

We then evaluated the green chemistry metrics and profitability of the electrochemical synthesis of benzylidene acetone from benzyl alcohol, as presented in this study. Specifically, we calculated key green chemistry indicators, including atom economy (AE), environmental factor (*E*-factor), and carbon efficiency (CE). Detailed calculation procedures for these metrics are provided in Note S2 (ESI).† The results from the electrochemical synthesis of benzylidene acetone show a high AE of 89%, a low *E*-factor of 0.71, and a high CE of 74%, suggesting that this synthesis method is potentially green and sustainable. To evaluate the economic market potential of sustainable benzylidene acetone electrosynthesis, a techno-economic analysis (TEA) was conducted (Fig. S31, ESI†).[16,49] The results indicate that the profit per ton of benzylidene acetone from this electrocatalytic technology can reach $936 (marked as a white star in Fig. 5e) and further reach $1009 when including the benefit of hydrogen (Note S3, ESI†), demonstrating the economic potential of this technique.

Paired benzylidene acetone electroreduction reaction

The obtained α,β-unsaturated ketones can enhance their added value through selective reduction to saturated ketones/alcohols.[50,51] In this system, α,β-unsaturated ketones are produced at the anode, and H_2 is the cathode product. We sought to further enhance the economic value by substituting the cathodic hydrogen evolution reaction (HER) with electroreduction of α,β-unsaturated ketones that are produced at the anode. Based on this concept, we designed a coupling reaction system involving electrosynthesis of benzylidene acetone at the anode and electroreduction of benzylidene acetone to benzylacetone at the cathode (Fig. 6a), aiming for the simultaneous preparation of high-value chemicals at both electrodes.

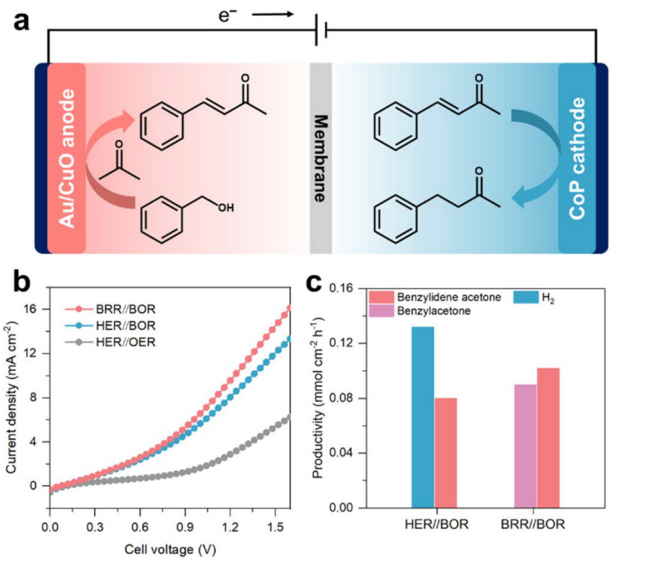

Fig. 6 (a) Schematic illustration of the coupling reaction system. (b) LSV curves of the HER//OER system, HER//BOR system and BRR//BOR system at a scan rate of 10 mV s^{-1}. (c) Productivities of different products in the three electrocatalytic systems at a cell voltage of 1.5 V.

Leveraging the excellent catalytic performance of Au/CuO for the BOR and CoP for the benzylidene acetone reduction reaction (denoted as BRR, Fig. S32, ESI†), we established an electrolytic system for co-producing benzylidene acetone (anode) and 4-phenylbutan-2-one (cathode) in a separate H-type quartz cell. Note that benzylidene acetone at the cathode is externally added, and the product at the anode does not cross the membrane to the cathode. The three coupling systems are denoted as HER//OER, HER//BOR and BRR//BOR, respectively. As shown in Fig. 6b, the current density of BRR//BOR is higher than that of HER//BOR and HER//OER. We then compared the product distribution and productivities in the HER//BOR and BRR//BOR coupling systems with the same electricity input (a constant potential of 1.5 V). As shown in Fig. 6c, for the HER//BOR system, the H_2 productivity was 0.13 mmol cm^{-2} h^{-1}. Additionally, benzylidene acetone was obtained at the anode with a productivity of 0.08 mmol cm^{-2} h^{-1} and an FE of 63% (Fig. S33, ESI†), showcasing the advantage of co-producing a high value-added product and H_2 fuel compared with traditional water electrolysis. For the BRR//BOR system, benzylidene acetone productivity reaches 0.1 mmol cm^{-2} h^{-1}, which is 1.3-fold higher than that of the HER//BOR system. Moreover, the productivity of 4-phenylbutan-2-one is 0.09 mmol cm^{-2} h^{-1}, and the FE is 70% (Fig. S34, ESI†), indicating that the co-production of benzylidene acetone and benzylacetone by electrocatalysis was realized.

Conclusions

In summary, we realize one-step electrosynthesis of benzylideneacetones and 2-phenylmethylene cyclohexanone *via* tandem

reactions. This approach couples selective electrooxidation of benzylic alcohols to the corresponding benzaldehydes over a cooperative Au/CuO catalyst with the spontaneous aldol condensation between the aldehyde and the ketone. We reveal that benzyl alcohol can be enriched at the Au/CuO interface and selectively oxidized by OH* generated on Au, playing a pivotal role in producing benzaldehyde as a crucial intermediate for the subsequent aldol condensation. Moreover, the tandem strategy demonstrates wide substrate applicability in the synthesis of diverse α,β-unsaturated ketones. As proof of concept, we realized the one-step electrosynthesis of benzylidene acetone at ampere-level current with a productivity of 9.5 mmol h^{-1} using a homemade membrane-free flow electrolyzer. Simultaneously, the cathodic H_2 productivity is 0.4 L h^{-1} with an energy consumption of only 3.2 kWh Nm^{-3} H_2. The calculations of key green chemistry metrics, such as AE, *E*-factor, and CE, indicate that this method could offer a green approach for producing benzylidene acetone. Furthermore, we integrated the electrosynthesis of benzylidene acetone at the anode with its electroreduction to the saturated ketone (4-phenylbutan-2-one) at the cathode, thereby enhancing electron economy, energy efficiency, and reaction integrity. This study showcases the potential for integrating electro-catalysis and thermo-catalysis in a single tandem reactor, offering implications for synthesizing more value-added chemicals.

Author contributions

Yifan Yan: conceptualization, methodology, writing – original draft, writing – review & editing, visualization, validation, formal analysis, investigation, and data curation. Xi Cai: visualization, validation, formal analysis, investigation, and data curation. Jiangrong Yang: visualization, validation, formal analysis, investigation, and data curation. Yu Fu: formal analysis and data curation. Qiwei Shi: formal analysis and data curation. Pengjie Hao: formal analysis and data curation. Hua Zhou: formal analysis, resources, data curation and investigation. Zhenhua Li: conceptualization, methodology, writing – review & editing, supervision and project administration. Mingfei Shao: conceptualization, supervision and project administration. Haohong Duan: conceptualization, methodology, writing – review & editing, supervision and project administration.

Data availability

The data that support the plots within the manuscript and other findings of this study are available from the corresponding author upon reasonable request.

Conflicts of interest

There are no conflicts to declare.

Acknowledgements

This work was financially supported by the National Key R&D Program of China (2022YFB4002700), the National Natural Science Foundation of China (22325805, 22090031, 22108008, and 22288102), the Young Elite Scientist Sponsorship Program by CAST (2021QNRC001) and the Fundamental Research Funds for the Central Universities (buctrc202011).

References

1 S. Zhang, H. Neumann and M. Beller, *Chem. Soc. Rev.*, 2020, **49**, 3187–3210.
2 S. Ren, F. Zhang, A. Xu, Y. Yang, M. Zheng, X. Zhou, Y. Fu and Y. Wang, *Nat. Commun.*, 2019, **10**, 1934.
3 A. Dhakshinamoorthy, M. Opanasenko, J. Čejka and H. Garcia, *Catal. Sci. Technol.*, 2013, **3**, 2509–2540.
4 Z. Zhang, Y. Wang, M. Wang, J. Lu, C. Zhang, L. Li, J. Jiang and F. Wang, *Catal. Sci. Technol.*, 2016, **6**, 1693–1700.
5 B. Spinello, Z. Strong, E. Ortiz, M. Evarts and M. Krische, *ACS Catal.*, 2023, **13**, 10976–10987.
6 H. Fan, Y. Yang, J. Song, G. Ding, C. Wu, G. Yang and B. Han, *Green Chem.*, 2014, **16**, 600–604.
7 H. Zou, Z. Wang, D. Guo, L. Zhang, S. Wang and X. Zhu, *Dalton Trans.*, 2024, **53**, 267–275.
8 H. Fan, Y. Yang, J. Song, G. Ding, C. Wu, G. Yanga and B. Han, *Green Chem.*, 2014, **16**, 600–604.
9 S. Tomer and H. Soni, *Catal. Sci. Technol.*, 2019, **9**, 6517–6531.
10 S. Zhai, W. Zhou, X. Dai, S. Yang, J. Qian, F. Sun, M. He and Q. Chen, *ChemistrySelect*, 2018, **3**, 11284–11292.
11 Z. Zhang, Y. Wang, M. Wang, J. Lu, C. Zhang, L. Li, J. Jiang and F. Wang, *Catal. Sci. Technol.*, 2016, **6**, 1693–1700.
12 H. Zhou, Y. Ren, Z. Li, M. Xu, Y. Wang, R. Ge, X. Kong, L. Zheng and H. Duan, *Nat. Commun.*, 2021, **12**, 4679.
13 Z. Li, X. Li, H. Zhou, Y. Xu, S. Xu, Y. Ren, Y. Yan, J. Yang, K. Ji, L. Li, M. Xu, M. Shao, X. Kong, X. Sun and H. Duan, *Nat. Commun.*, 2022, **13**, 5009.
14 Y. Yan, P. Hao, Y. Fu, W. Chen, Q. Shi, H. Zhou, X. Kong, Z. Li, M. Shao and X. Duan, *AIChE J.*, 2024, e18370.
15 Y. Yan, Q. Wang, P. Hao, H. Zhou, X. Kong, Z. Li and M. Shao, *ACS Appl. Mater. Interfaces*, 2023, **15**, 23265–23275.
16 Y. Lum, J. Huang, Z. Wang, M. Luo, D. Nam, W. Leow, B. Chen, J. Wicks, Y. Li, Y. Wang, C. Dinh, J. Li, T. Zhuang, F. Li, T. Sham, D. Sinton and E. Sargent, *Nat. Catal.*, 2020, **3**, 14–22.
17 Y. Yan, H. Zhou, S. Xu, J. Yang, P. Hao, X. Cai, Y. Ren, M. Xu, X. Kong, M. Shao, Z. Li and H. Duan, *J. Am. Chem. Soc.*, 2023, **145**, 6144–6155.
18 J. Wu, L. Xu, Z. Kong, K. Gu, Y. Lu, X. Wu, Y. Zou and S. Wang, *Angew. Chem.*, 2023, **135**, e202311196.
19 Y. Wu, W. Chen, Y. Jiang, Y. Xu, B. Zhou, L. Xu, C. Xie, M. Yang, M. Qiu, D. Wang, Q. Liu, Q. Liu, S. Wang and Y. Zou, *Angew. Chem.*, 2023, **135**, e202305491.

20 W. Chen, Y. Wu, Y. Jiang, G. Yang, Y. Li, L. Xu, M. Yang, B. Wu, Y. Pan, Y. Xu, Q. Liu, C. Chen, F. Peng, S. Wang and Y. Zou, *J. Am. Chem. Soc.*, 2024, **146**, 6294–6306.
21 Y. Wu, J. Zhao, C. Wang, T. Li, B. Zhao, Z. Song, C. Liu and B. Zhang, *Nat. Commun.*, 2023, **14**, 3057.
22 W. Bing, L. Zheng, S. He, D. Rao, M. Xu, L. Zheng, B. Wang, Y. Wang and M. Wei, *ACS Catal.*, 2017, **8**, 656–664.
23 M. Sharma, B. Das, M. Sharma, B. Deka, Y. Park, S. Bhargava and K. Bania, *ACS Appl. Mater. Interfaces*, 2017, **9**, 35453–35462.
24 R. Poreddy, C. Engelbrekt and A. Riisager, *Catal. Sci. Technol.*, 2015, **5**, 2467–2477.
25 M. Marelli, A. Jouve, A. Villa, R. Psaro, A. Balerna and L. Prati, *J. Phys. Chem. C*, 2019, **123**, 2864–2871.
26 N. Bisht, S. Mehta and N. Sahoo, *Dalton Trans.*, 2021, **50**, 5001–5010.
27 Z. Fang, P. Zhang, M. Wang, F. Li, X. Wu, K. Fan and L. Sun, *ACS Sustainable Chem. Eng.*, 2021, **9**, 11855–11861.
28 Z. Li, Y. Yan, S. Xu, H. Zhou, M. Xu, L. Ma, M. Shao, X. Kong, B. Wang, L. Zheng and H. Duan, *Nat. Commun.*, 2022, **13**, 147.
29 Y. Zhang, B. Zhou, Z. Wei, W. Zhou, D. Wang, J. Tian, T. Wang, S. Zhao, J. Liu, L. Tao and S. Wang, *Adv. Mater.*, 2021, **33**, 2104791.
30 M. Jiang, P. Sun, J. Zhao, L. Huo and G. Cui, *Sensors*, 2019, **19**, 5055.
31 Y. Deng, A. Handoko, Y. Du, S. Xi and B. Yeo, *ACS Catal.*, 2016, **6**, 2473–2481.
32 V. Kobychev, V. Orel, N. Vitkovskaya and B. Trofimov, *Dokl. Chem.*, 2014, **457**, 1.
33 B. Mao, P. Sun, Y. Jiang, T. Meng, D. Guo, J. Qin and M. Cao, *Angew. Chem.*, 2020, **132**, 15344–15349.
34 P. Rodriguez, Y. Kwon and M. Koper, *Nat. Chem.*, 2012, **4**, 177–182.
35 G. Zhang, Z. Zhao, D. Cheng, H. Li, J. Yu, Q. Wang, H. Gao, J. Guo, H. Wang, G. Ozin, T. Wang and J. Gong, *Nat. Commun.*, 2021, **12**, 5745.
36 G. Li, G. Han, L. Wang, X. Cui, N. Moehring, P. Kidambi, D. Jiang and Y. Sun, *Nat. Commun.*, 2023, **14**, 525.
37 Z. Han, D. Han, Z. Chen, J. Gao, G. Jiang, X. Wang, S. Lyu, Y. Guo, C. Geng, L. Yin, Z. Weng and Q. Yang, *Nat. Commun.*, 2022, **13**, 3158.
38 Y. Zhang, J. Wang, X. Yu, D. Baer, Y. Zhao, L. Mao, F. Wang and Z. Zhu, *ACS Energy Lett.*, 2018, **4**, 215–221.
39 S. Engbers and J. Klein, *ChemPhysChem*, 2023, **24**, e202200475.
40 T. Matsuyama, T. Yatabe, T. Yabe and K. Yamaguchi, *ACS Catal.*, 2022, **12**, 13600–13608.
41 Z. Li, L. Luo, M. Li, W. Chen, Y. Liu, J. Yang, S. Xu, H. Zhou, L. Ma, M. Xu, X. Kong and H. Duan, *Nat. Commun.*, 2021, **12**, 6698.
42 X. Guo, H. Fu, J. Yang, L. Luo, H. Zhou, M. Xu, X. Kong, M. Shao, H. Duan and Z. Li, *ACS Catal.*, 2023, **13**, 13528–13539.
43 Z. Xia, C. Ma, Y. Fan, Y. Lu, Y. Huang, Y. Pan, Y. Wu, Q. Luo, Y. He, C. Dong, S. Wang and Y. Zou, *ACS Catal.*, 2024, **14**, 1930–1938.
44 P. Zou, X. Lv, S. Tao, J. Wu, H. Wang, X. Wei, T. Wang, B. Zhou, Y. Lu, T. Frauenheim, X. Fu, S. Wang and Y. Zou, *Adv. Mater.*, 2022, **34**, 2204089.
45 A. Garcia, M. Kolb, C. Sanchez, J. Vos, Y. Birdja, Y. Kwon, G. Tremiliosi-Filho and M. Koper, *ACS Catal.*, 2016, **6**, 4491–4500.
46 Y. Guo, R. Hu, X. Zhou, J. Yu and L. Wang, *Appl. Surf. Sci.*, 2019, **479**, 989–996.
47 T. Bligaard, J. Nørskov, S. Dahl, J. Matthiesen, C. Christensen and J. Sehested, *J. Catal.*, 2004, **224**, 206–217.
48 J. Wang, F. Xu, H. Jin, Y. Chen and Y. Wang, *Adv. Mater.*, 2017, **29**, 1605838.
49 N. Meng, J. Shao, H. Li, Y. Wang, X. Fu, C. Liu, Y. Yu and B. Zhang, *Nat. Commun.*, 2022, **13**, 5452.
50 F. Beltran, E. Bergamaschi, I. Funes-Ardoiz and C. Teskey, *Angew. Chem.*, 2020, **132**, 21362–21368.
51 X. Li, L. Li, Y. Tang, L. Zhong, L. Cun, J. Zhu, J. Liao and J. Deng, *J. Org. Chem.*, 2010, **75**, 2981–2988.